Characterization of the External Surface of Silicalites Employing Electron Paramagnetic Resonance[†,||]

Zhiqiang Liu,[‡,#] M. Francesca Ottaviani,[§] Lloyd Abrams,[⊥] Xuegong Lei,[‡] and Nicholas J. Turro*[,‡]

Department of Chemistry, Columbia University, New York, New York 10027, Institute of Chemical Sciences, University of Urbino, 61029 Urbino, Italy, and Central Research and Development Department, E. I. duPont de Nemours and Co., Inc., Wilmington, Delaware 19880

Received: February 17, 2004; In Final Form: April 6, 2004

Sensitive and structurally specific methods for investigating silicalite external surface have been developed using electron paramagnetic resonance (EPR). The absorption of an EPR silent probe ortho-methyldibenzyl ketone (oMeDBK) (**4** in Scheme 1) on the external surface of a series of monodisperse silicalite crystals was studied using an initially coadsorbed EPR active nitroxide probe. The displacement of the initially adsorbed nitroxide probe by coadsorbed oMeDBK shows that the adsorbate molecules first adsorb on stronger binding sites characterized by slow rotational motion of the probe (broad EPR lines) and after the stronger sites are saturated, the displaced EPR probe molecules adsorb on weaker binding sites characterized by fast rotational motion of the probe (narrow EPR lines). The transition point from slow to fast rotational motion provides a quantitative measurement of the stronger binding sites on the silicalite external surface area and the external surface area of silicalite crystals. The adsorption strength is molecular structure-dependent, and polar functional groups provide significant contribution to the binding strength. Sequential adsorption of ^{14}N and ^{15}N spin-labeled nitroxides shows the presence of the dynamic exchange between the adsorbates on the strong binding sites and those in solution or on the weak binding sites, while concurrent coadsorption of ^{14}N and ^{15}N spin-labeled nitroxides provides another sensitive means of studying the molecular structural dependence of the binding strength.

Introduction

The MFI family of zeolites has found wide application in shape-selective catalysis and the separation sciences.[1,2] The crystal structure of MFI zeolites is characterized by a framework of linked tetrahedra, each consisting of SiO_4 or AlO_4^- units. ZSM-5 zeolites are the aluminum-containing members of the MFI family, while silicalites are the members composed entirely of SiO_4 tetrahedra. MFI zeolites possess two sets of channel systems, a straight channel system running through the crystals in the direction of [010] with a pore size of about 5.3 × 5.6 Å and a sinusoidal channel system running along the direction of [100] with a dimension of 5.1 × 5.5 Å (Figure 1).[3] The intersection of the two sets of channels creates a supercage cavity with a diameter about 9 Å.

The surfaces of MFI zeolites can be separated into two parts: (1) the internal surface comprising the walls of the channels and the intersections and (2) the external surface comprising the pore openings and the framework surface between the pore openings on the outside of the crystals (Figure 1). The external surface accounts for only a very small percentage of the total surface area for typical MFI zeolite crystals with sizes of ca. 1 μm. For example, the external surface areas (ESA) account for only 4.5% and 0.26% of the total surface area, for ZSM-5 zeolite crystals with sizes of ca. 2 μm and 10 μm, respectively.[4]

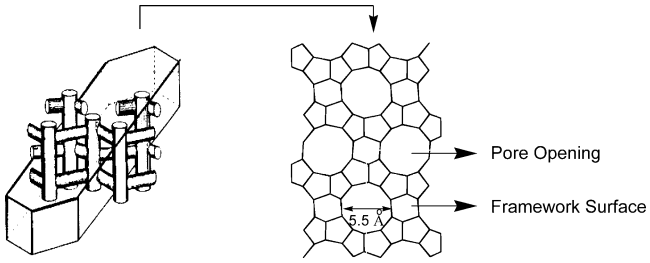

Figure 1. A MFI zeolite crystal (left), channel structures (left), and external surface (right, exemplified by the [010] surface). The channels are drawn superimposed onto the crystals for illustration purpose only and are not drawn according to scale. The external surface consists of pore openings and framework surface.

The zeolite external surface area (ESA) is an important parameter that affects its catalytic performance. Applications of zeolites typically begin with the initial adsorption of molecules (from the gas phase or the liquid phase) on the external surface of a zeolite crystal followed by diffusion on the external surface and sieving of the molecules into the internal surface. The size/shape selective catalysis can be classified into two major categories: (1) diffusion-controlled size/shape selectivity depending on the relative rates of diffusion of reagents into the internal surface or products out of the internal surface and (2) transition-state selectivity in the confined environment of the zeolite channels and their intersections.[1] In either case, the size/shape selective reactions are mainly associated with the

[†] Part of the special issue "Richard Bersohn Memorial Issue".
[||] E. I. duPont de Nemours and Co. Contribution No. 8538.
* Address correspondence to this author. E-mail: njt3@columbia.edu.
[‡] Columbia University.
[§] University of Urbino.
[⊥] E. I. duPont de Nemours and Co.
[#] Present address: Columbia Genome Center, Columbia University, New York, NY 10032.

10.1021/jp049275h CCC: $27.50
Published on Web 05/18/2004

reactions that take place in the zeolite internal surface. Reactions on the external surface typically do not proceed in a size/shape selective manner. Therefore, assuming a comparable catalytic reactivity of the reagents on the internal and external surface, zeolite crystals with larger crystal sizes and consequently smaller ESA per unit mass will possess higher catalytic size/shape selectivity. However, the ESA is directly proportional to the concentration of the pore openings, which in turn affects the velocity of diffusion of reagent molecules into the channels or the product molecules out of the channels. As a result, the size/shape selective catalysis in the internal surface proceeds at a lower rate for larger crystals because of limitations on diffusion of the guest molecules, and side reactions could become more pronounced when the desired reaction is diffusionally retarded. Therefore, the ESA of an MFI zeolite is a parameter of great industrial importance and should be measured and optimized for various applications.

Various methods have been developed for the measurements of zeolite ESA, including the Langmuir isotherm[5,6] and BET isotherm.[7] In a typical Langmuir or BET isotherm analysis of solid-surface area, the experiment is conducted using nitrogen adsorption at low temperature (e.g., 77 K).[7] Nitrogen, with a size ca. 3 Å along its long axis, is small enough to penetrate MFI zeolite pores, and therefore typical isotherm analysis offers a measurement of the total zeolite surface area, including both internal and external surfaces. Since the extent of internal surface area is typically much greater than the ESA, conventional nitrogen isotherm measurements provide essentially no information on the ESA. Modifications have been made to the isotherm methods to measure the zeolite ESA only. One method employs the adsorption of adsorbate molecules that are larger than the pore openings, and another method uses conventional nitrogen adsorption isotherm after plugging the pores with molecules of appropriate size, hence called filled-pore isotherm.[4] Non-Langmuir/BET type isotherms for the zeolite ESA determination have also been developed, and these methods include (a) an adsorption kinetics method in which the speed of adsorption on the external surface and internal surface is exploited when the size of the adsorbate molecule is such that it can access both the internal and external surfaces;[8] (b) measurements in which the volume of adsorbed nitrogen is plotted against the statistical film thickness (t-plot);[9] (c) simple geometrical analysis using scanning electron microscopy (SEM); and (d) mercury porosimetry.[10,11] These methods for the measurement of the zeolite ESA have been the subject of many publications including reviews[8,12,13] and have been used in various combinations on zeolites including ZSM-5 zeolites[4,14,15] and others.[16] These methods for determining the zeolite ESA have shown a varying degree of success depending on the specific systems. One of the major constraints is that the low sensitivity of the conventional adsorption isotherm makes it unsuitable for the most commonly used ZSM-5 zeolite crystals whose ESA typically accounts for only a small percentage of the total surface area. Another typical constraint is the necessity of mathematical disentangling of the ESA from the internal surface area, particularly for adsorption kinetics and t-plot methods.

Some efforts have been made in the literature to develop a sensitive method for the exclusive characterization of the zeolite external surface. The exclusive characterization of the external surface is typically achieved using an adsorbate species that has a molecular size larger than the pore openings and, therefore, adsorbs exclusively on the external surface. An enhancement in sensitivity is typically achieved by using highly sensitive spectroscopic methods, such as magnetic resonance. The ESA of a superhigh-silica ZSM-5 zeolite was determined using electron paramagnetic resonance (EPR) with TEMPO as the probe molecule.[17] Li and Turro et al.[18,19] studied the external surface of ZSM-5 zeolites by adsorbing various probe molecules exclusively on the external surface and subsequently measuring the rotational mobility of the probe molecules spectroscopically (^{2}H NMR and EPR) at different surface coverage. The study also suggested that the pore openings are stronger binding sites for organic molecules such as ortho-methyl dibenzyl ketone (oMeDBK) and nitroxides than the framework surface. Adsorption of oMeDBK occurs at the pore openings at low adsorbate loadings and further extends to the framework surface at high loadings. Ottaviani et al. studied the evolution of EPR spectra of nitroxide probes adsorbed on silicalite and ZSM-5 zeolite external surfaces.[20] By increasing the loading of coadsorbates such as oMeDBK, the nitroxide EPR spectra changed from that characteristic of slow rotational motions of the nitroxide probe molecules to that characteristic of fast rotational motions. On the basis of measurements on a silicalite sample and a ZSM-5 sample, both having polydisperse crystal sizes, a preliminary conclusion was reached that the loading of coadsorbed species which is required to show a transition in the nitroxide EPR spectra from slow rotational motion to fast rotational motion is directly proportional to the zeolite ESA. This postulate is further examined in detail in the current research, employing seven monodisperse silicalite crystals with monodisperse crystal size ranges over an order of magnitude. The use of monodisperse crystals leads to more homogeneous properties related to the external surface and more reproducible sampling. The presence of aluminum in ZSM-5 zeolites potentially provides strong binding sites on the external surface, and the distribution of aluminum in the crystal and on the external surface of the crystal is influenced by subtle differences in the synthesis recipes and procedures. The use of silicalites rather than ZSM-5 zeolites helps avoid the complications introduced by aluminum to the binding of organic adsorbates on the zeolite external surface.

Experimental Section

Instrumentation. ^{1}H NMR and ^{13}C NMR measurements were performed on Bruker NMR spectrometers at 400 (or 300) MHz and 100 (or 75) MHz, respectively. Gas chromatography (GC) was performed on an HP5890 gas chromatograph using an HP-5 capillary column. Gas chromatography/mass spectrometry (GC/MS) was performed on a Varian Star 3900 GC/MS instrument using electron ionization. FAB-MS was recorded in the positive ion mode using 3-nitrobenzyl alcohol as the matrix on a JMS−HX110A/110A tandem mass spectrometer. Continuous wave EPR (CW-EPR) measurements were carried out on an X-band Bruker EMX EPR spectrometer. X-ray diffraction (XRD) measurements were carried out on a Scintag X2 X-ray diffractometer operating at 45 KV and 35 mA. Scanning electron microscopy (SEM) images were taken on a JEOL JSM-5600 electron microscope.

Reagents. All reagents were obtained from Aldrich and used as received, unless otherwise noted. Amorphous silica in the form of fumed silica gel was obtained from Degussa (Aerosil 200).

Synthesis of Monodisperse Silicalite Crystals of Various Crystal Sizes. *A.* Syntheses of silicalite crystals with sizes less than 1 μm were carried out at 98 °C in polypropylene bottles using clear homogeneous alcoholic solutions with hydrolyzed tetraethoxysilane (TEOS) as the source of SiO_2. The general molar compositions of the synthesis mixtures are given in Table 1.

TABLE 1: The Compositions of the Reaction Mixtures (a TPABr:b TPAOH:0.1 Na_2O:25 SiO_2:c H_2O:100 EtOH), Aging and Heating Times, and Conversions for the Syntheses of Silicalite Crystals with Sizes Less than 1 μm

run	a	b	c	aging (h)	heating time (h)	conversion (%)
S1	3.0	6.0	480	25	67	75
S2	0	3.0	480	19	100	65
S3	0	3.0	1500	17	96	61

TABLE 2: The Compositions of the Reaction Mixtures (a TPABr:1.4 Na_2O:100 SiO_2:b H_2O), Aging and Heating Times, and Conversions for the Syntheses of Silicalite Crystals with Sizes in the Range of 1 and 10 μm

run	a	b	aging (h)	heating program	conversion (%)
S4	16	1061	12	start at 45 °C, 0.3 °C/min ramp to 170 °C, hold for 47 hours	70
S5	8	1000	6	start at 45 °C, 0.3 °C/min ramp to 170 °C, hold for 77 hours	60

The reaction mixture was prepared by mixing tetrapropylammonium bromide (TPABr), tetrapropylammonium hydroxide (TPAOH), sodium hydroxide, TEOS, deionized water, and ethanol (EtOH). After aging the mixture at room temperature, the reaction was carried out by refluxing at 98 °C for the specified period of time and then the mixture was cooled to room temperature. The colloidal mixture was transferred to polypropylene centrifuge tubes and the solid was separated from the liquid using ultrahigh centrifugation (13800×g for S1 and 27000×g for S2 and S3). The solid was dispersed in deionized water, sonicated, and reseparated from water using centrifugation. This dispersion/sonication/centrifugation cycle was repeated until the pH of the aqueous layer was lower than 8. This was achieved typically in three cycles. The solid was dried at 130 °C and then calcined in an aerated furnace, with the following as a representative temperature program: 300 °C for 2 h, 400 °C for 2 h, and 500 °C until the solid turned white.

B. Syntheses of silicalite crystals with sizes in the range of 1−10 μm were carried out following a published procedure with modifications, using amorphous fumed silica gel as the source of SiO_2 in heterogeneous systems.[21]

The batch compositions in molar ratios are given in Table 2.

TPABr, NaOH, SiO_2 (in the form of fumed silica gel), and deionized water were mixed in a polypropylene beaker. The slurry was then transferred to PTFE-lined steel autoclaves. After aging, the reaction was carried out in a static condition under autogenous pressure following the temperature program as detailed in Table 2. After the desired period of reaction time, the reaction was quenched by cooling the autoclaves under cold water. The product was then dispersed in deionized water and sonicated. The crystalline solid was then separated from the supernatant containing unreacted gel by simple gravitational sedimentation or light centrifugation, followed by decantation. The sonication and separation cycle was repeated between 5 and 10 times, until the pH was less than 8 and the supernatant was clear, indicating the complete removal of unreacted gel. The crystalline solid was then calcined according to the procedure detailed in the previous section.

C. Silicalite crystals with sizes in the range of 10−100 μm were synthesized using neutral or even slightly acidic compositions containing fluoride in the form of a salt or hydrofluoric acid. The fluoride plays a mineralizing role, as OH^- does in conventional alkaline systems.[22] The benefit of using F^- includes the formation of large crystals, ca. 100 μm, with much fewer surface defects as compared to the crystals prepared using an alkaline medium.[22]

TABLE 3: The Compositions of the Reaction Mixtures (a HF:b NaF:c NaCl:1.25 TPABr:10 SiO2:330 H_2O), Aging and Heating Times, and Conversions for the Syntheses of Silicalite Crystals with Sizes in the Range of 10−100 μm

run	a	b	c	aging (h)	heating program	conversion (%)
S6	0	7	3	16	start at 45 °C, 0.3 °C/min ramp to 170 °C, hold for 91 hours	59
S7	0.25	0.75	0.25	0	start at 45 °C, 0.3 °C/min ramp to 170 °C, hold for 270 hours	88

The syntheses of silicalite crystals were based on published procedures,[23,24] using the molar ratios given in Table 3.

The reagents were mixed together in a polypropylene beaker. The slurry was transferred to PTFE-lined steel autoclaves and (after aging in sample S6) the reaction mixture was heated according to the temperature program described in Table 3. The reaction was quenched by cooling the autoclaves using tap water. The product was dispersed in deionized water and sonicated. The solid can be separated from the aqueous layer by simple decantation. The dispersion/sonication/ decantation cycle was repeated ca. 10 times until the aqueous layer showed a pH less than 8 and became clear, indicating the absence of unreacted gel. The calcinations were carried out using the following program. After drying at 130 °C, the solid was heated to 300 °C and then the temperature was increased at 20 °C/h until 400 °C and held at 400 °C for more than 12 h. The temperature was then raised at a 20 °C/h ramp to 500 °C and held at 500 °C until the crystals turned white.

Syntheses of Nitroxide Probe Molecules and Coadsorbates. 4-Oxo-2,2,6,6-tetramethyl-1-piperidinyloxy-^{15}N (4-oxo-TEMPO-^{15}N, **1-^{15}N**). The precursor 4-oxo-2,2,6,6-tetramethyl-1-piperidine-^{15}N for **1-^{15}N** was synthesized following a published procedure using ammonium-^{15}N sulfate (98+ at. %) in 66% yield.[25] **1-^{15}N** was prepared by oxidizing the amine precursor following a published procedure in 39% yield.[26] GC (>98% pure). GC/MS (EI) *m/z* (rel intensity): 171 (M^+, 100), 172 (39), 157 (24), 141 (35), 115 (48), 83 (61).

2,2,6,6-Tetramethyl-4-[(diphenylacetyl)oxy]-1-piperidinyloxy (**3**) was synthesized following a published procedure for esterification at room temperature using 4-hydroxy-2,2,6,6-tetramethyl-1-piperidinyloxy-^{15}N and diphenylacetic acid in 66% yield.[27] It was recrystallized using ethyl acetate. MS (FAB+): 366.2 $(M - H)^+$, 368.2 $(M + H)^+$.

2,2,6,6-Tetramethyl-4-[(diphenylacetyl)oxy]-1-piperidinyloxy-^{15}N (**3-^{15}N**) was synthesized following the procedure for **3**, using 4-hydroxy-2,2,6,6-tetramethyl-1-piperidine-^{15}N, the latter prepared by a reduction of **1-^{15}N** using sodium borohydride in 94% yield. MS (FAB+): 367.2 $(M - H)^+$, 369.2 $(M + H)^+$.

1-Phenyl-3-o-tolyl-propan-2-one (oMeDBK, **4**),[19] 1,3-di-*o*-tolyl-propan-2-one (*o*,*o*′-diMeDBK, **5**),[20] 1,3-di-*p*-tolyl-propan-2-one (*p*,*p*′-diMeDBK, **6**),[28] and 1,2-bis(2-methylphenyl)ethane **(7)**[20] were prepared following published procedures.

Preparation of Silicalite Samples Loaded with Adsorbates. The calcined silicalite samples were activated at 500 °C for at least 1 h in an aerated furnace and then were placed in a desiccator and allowed to cool to room temperature before use. Gravimetric analysis was used to confirm the removal of residual water in the activated silicalite samples.

2,2,4-Trimethyl-pentane (isooctane) was chosen as the preferred solvent for the silicalite sample preparation because of several advantageous properties.[29] Isooctane's kinetic diameter is larger than the ZSM-5/silicalite pore openings and thus isooctane does not enter the zeolite internal void.[30] The

combination of exclusion from the internal void and isooctane's low boiling point (99.2 °C) make it easy to remove under vacuum after the adsorbates are loaded. Isooctane is a saturated hydrocarbon with very low polarity (polarity index = 0.1 on the Snyder scale as compared to *n*-hexane at 0.1, toluene at 2.4, *o*-xylene at 2.5, and methyl ethyl ketone at 4.7),[31] and consequently is not expected to significantly compete for binding sites with the adsorbate probes employed in this study.

Adsorbate molecules were loaded onto the silicalite external surface by mixing stock solutions of an appropriate amount with cold and dry silicalite samples. The loadings are expressed in the unit of millimolal (m*m*). In an airtight container, the slurry was stirred magnetically until the adsorption reached equilibrium, that is, the ratio of adsorbed fraction versus the fraction in solution no longer changed over time. The equilibrium was typically achieved in less than 10 h. The progress toward equilibrium was followed by checking the concentration of adsorbates in the supernatant using UV or GC after centrifugation.

To obtain the dry loaded samples, the solvent was first removed under a gentle stream of an argon flow. The oMeDBK and TEMPO molecules were therefore forced to deposit onto the silicalite external surface. The dry silicalite samples thus loaded with adsorbate molecules were further dried and degassed under vacuum (ca. 5×10^{-4} Torr) in a quartz tube and then their EPR spectra were recorded.

The EPR spectra were recorded at room temperature (approximately 24 °C) using the lowest possible microwave power (~2.01 mW at 20 dB) and with modulation frequency at 100 kHz and modulation amplitude smaller than the narrowest line width in the spectra except for the proton hyperfine lines.

Results and Discussions

The seven silicalite samples synthesized are composed of monodisperse crystals with a range of sizes (Figure 2). The MFI crystal structures were confirmed using XRD (Supporting Information).

The ESA of the silicalite samples per unit mass was measured using mercury porosimetry (Table 4).[11]

The structures of the nitroxide probe molecules and coadsorbate molecules are shown in Scheme 1. All these nitroxides (**1**−**3** including their isotopomers) are based on the 2,2,6,6-tetramethylpiperidin-1-oxy structure (kinetic diameter = 11 Å), which adsorbs exclusively on the external surface of silicalite crystals.[32] The EPR silent coadsorbates **4**, **5**, and **7** possess *o*-xylyl moieties, which prevent the coadsorbate molecules from diffusing into the internal void and thus exclusively adsorb on the silicalite external surface.[20,29] The EPR silent coadsorbate **6** has a molecular cross section smaller than the cross section of the silicalite pore openings, and thus absorbs into and probes the silicalite internal surface.

Determination of Silicalite ESA Using Nitroxide EPR with Coadsorbates. The EPR spectra (Figure 3) of the nitroxide probe molecules (Scheme 1) on the silicalite external surface depend strongly on the amount of coadsorbed oMeDBK (**4**).

The nitroxide EPR spectra, with increasing loading of **4**, undergo a transition from broad lines to narrow lines. This observation is rationalized as shown in Figure 3. In the absence of **4**, the nitroxide probe molecules bind to the strong binding sites (pore openings) on the external surface and display reduced rotational mobility resulting in a broad line spectrum. As **4** is added to the system, the coadsorbed oMeDBK molecules compete with the adsorbed nitroxide probe for the strong binding sites and lead to partial displacement of the nitroxide probes from the strongly bound positions. As more **4** is added, more nitroxide probes are displaced. The nitroxide probes that are displaced to the framework of the external surface show increased rotational mobility, which is signaled by the appearance of a characteristic sharp three-line spectrum.

The critical loading of oMeDBK required to bring out the onset of the fast motion for the nitroxide probes is therefore expected to be a parameter directly proportional to the number

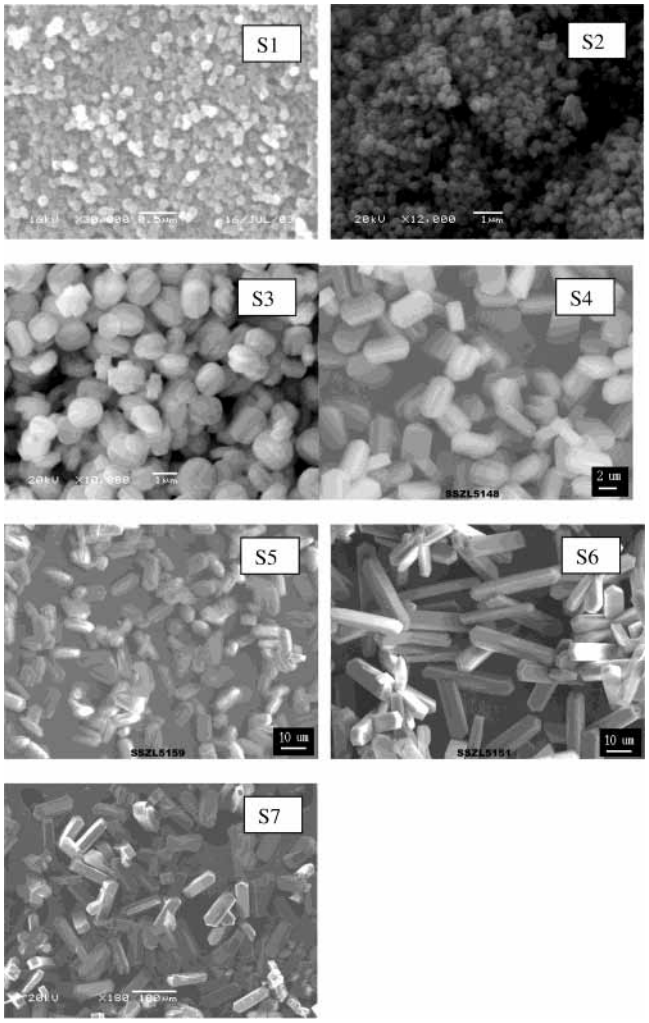

Figure 2. SEM images of synthetic silicalite samples with different crystal sizes.

TABLE 4: ESA Per Gram of Silicalite Crystal Measured by Mercury Porosimetry

silicalite	S1	S2	S3	S4	S5	S6	S7
ESA (m^2/g)	55.1	20.3	9.27	5.71	29.8	3.75	2.75

SCHEME 1: Structures of the Nitroxide Probe Molecules and Coadsorbate Molecules

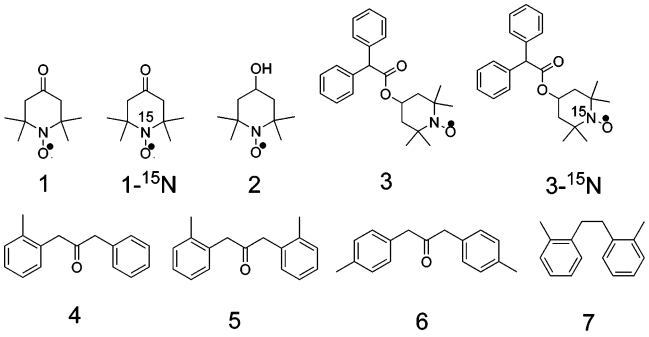

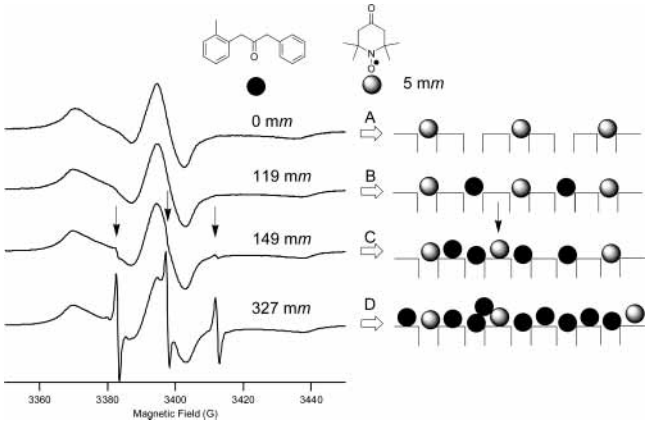

Figure 3. Molecular interpretation of adsorption on the external surface of silicalite (right) and corresponding EPR spectra (left). (A) Low loadings of nitroxide (light-shaded balls) lead to the adsorption on the strong binding sites (pore openings) only and the EPR spectra are characteristic of slow rotational motion. (B) Coadsorbed oMeDBK molecules (black-filled balls) favor the strong binding sites and up to a certain loading do not disturb the nitroxide probe molecules on the strong binding sites. (C) When the strong binding sites are fully occupied, oMeDBK displaces some nitroxide molecules from strong binding sites. Correspondingly, a fast motion component appears in the EPR spectrum (arrows). (D) At higher coverage, more nitroxides are displaced from the strong binding sites, resulting in a larger percentage of fast motion in the nitroxide EPR spectrum.

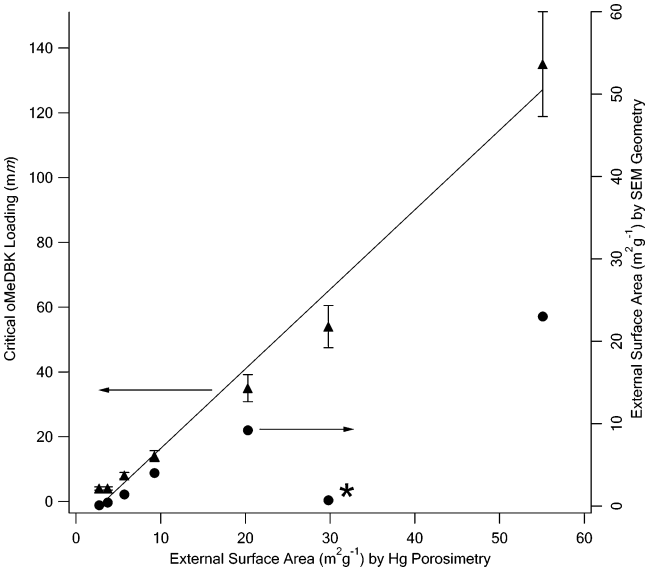

Figure 4. The critical loadings of **4** required to reach the onset of EPR fast motion of **1** (left ordinate), and the ESA determined using geometrical analysis of SEM photographs (right ordinate) as a function of ESA determined by mercury porosimetry analyses (abscissa) for all seven monodisperse silicalite crystals. Errors for the critical loadings of **4** were determined to be 12%. The straight line represents a linear fitting of the loadings to mercury porosimetry results ($R^2 = 0.99$). The star indicates the sample point where a significant aberration of SEM geometrical analysis takes place.

of binding sites, postulated as the number of pore openings, which in turn depends on the total ESA of a silicalite sample, assuming that the pore openings are similarly distributed in the various zeolite crystals. On this basis, the critical loading of oMeDBK which produces the onset of nitroxide fast motion can provide an accurate, fast, and selective measurement of the ESA of MFI crystals. Figure 4 shows the critical loadings of oMeDBK (**4**) required for the onset of the sharp component measured by the displacement of 4-oxo-TEMPO (**1**) on the seven silicalite samples examined plotted against their

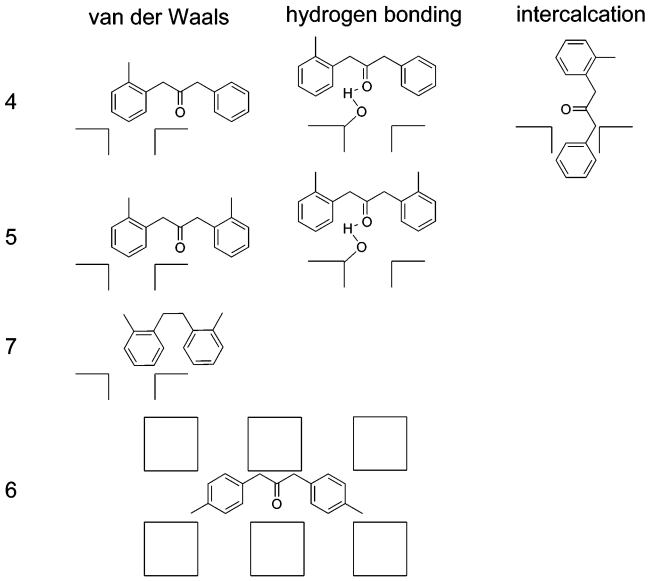

Figure 5. The expected adsorption patterns on silicalite surface of various coadsorbates employed in this study. **4**, **5**, and **7** absorb on silicalite external surface only and **6** absorbs on silicalite internal surface.

corresponding ESA measured using the established mercury porosimetry method. It can be determined that there exists an approximately linear relationship between the critical loadings of **4** and the ESA determined by mercury porosimetry. Thus, it can be concluded that the study of rotational mobility of nitroxide probes on silicalite external surface in the presence of coadsorbed oMeDBK can be used for the measurement of silicalite ESA. In principle, the absolute value of the ESA can be obtained provided that a precharacterized and calibrated silicalite sample is available as a standard. In addition, Figure 4 shows the ESA of silicalite crystals estimated using the geometrical analysis based on the SEM photographs. Comparing the ESA determined by SEM geometrical analysis and that determined by mercury porosimetry, it can be appreciated that the SEM method leads to a considerable underestimate (and sometimes significant aberration from the linearity, such as the point marked with a star symbol) of the ESA. These inaccuracies are due to the difficulties in quantifying the ESA of irregular and small crystals, in resolving and accounting for the complicated external surface structures on the nanometer scale, and in accounting for the contributions of impurities to the total ESA of a given sample. In contrast, the small sizes of molecular probes (less than 1 nm) such as **1** and **4** ensure that the contribution to the total ESA from those complications is accounted for, and the EPR method for ESA measurement is therefore more reliable than the geometrical analysis from SEM photographs.

Dependence of Binding Strength on the Molecular Structures of the Adsorbate Molecules on the Silicalite External Surface. The concept of competitive binding on the silicalite ESA was further exploited to unravel the dependence of binding strength on the molecular structures of the adsorbates.

As summarized in Figure 5 for the various coadsorbates, different adsorption patterns and strengths arise from different adsorbate structures. van der Waals interaction between the surface and the adsorbate is always present. In addition, the presence of the carbonyl group is expected to play a significant role in the adsorption of ketones at the zeolite surface, possibly through the hydrogen bonding between the carbonyl groups and the silanols at surface defect sites. The tolyl group of **4** is expected to contribute to the binding strength of oMeDBK on

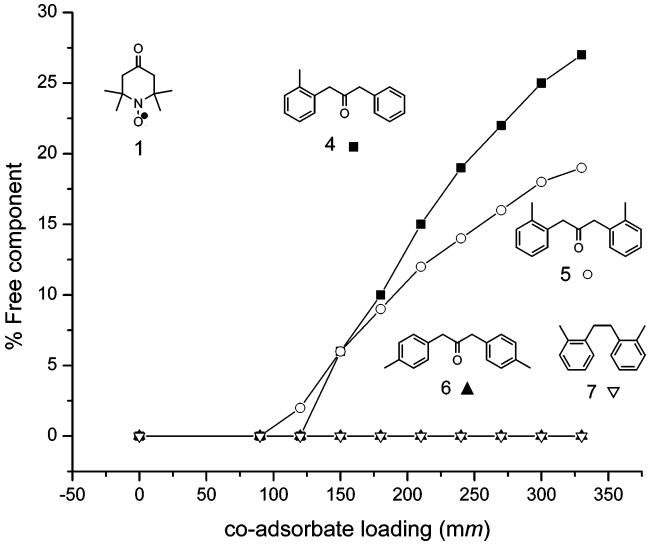

Figure 6. The percentage of nitroxide probes, **1**, in fast rotational motion as a function of the structures and loadings of the coadsorbate species **4**−**7**.

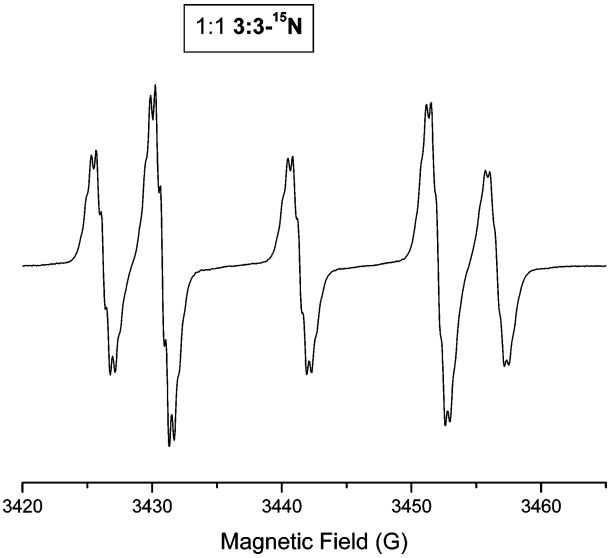

Figure 7. EPR spectrum of an equimolar mixture of ^{14}N (0.25 mM) and ^{15}N (0.25 mM) labeled nitroxides (**3** and **3-^{15}N**) in isooctane (deoxygenated). The superhyperfine couplings (∼0.4 G) are due to the interaction of the electron spin with protons in the nitroxide molecules.

the silicalite external surface.[19] The benzene ring has a kinetic diameter of 5.85 Å, just slightly smaller than the kinetic diameter of the MFI zeolite pores (∼6 Å).[33] The tight fit leads to enhanced dispersion interaction between the intercalated tolyl group and the channel walls because of increased contact and the interaction between the π electron cloud in the tolyl group and the electric field gradient, such as those provided by the surface defect sites.[34] The presence of one or more *o*-xylyl groups (kinetic diameter ∼6.8 Å) in **4**, **5,** and **7** prevent them from diffusing into the silicalite internal surface. Therefore, neither **5** nor **7** can intercalate into the pore openings. **6** is capable of diffusing into the pore openings and probes the silicalite internal surface.

To check the dependence of the binding strength on the molecular structure of the adsorbates with respect to the presence and distribution of methyl and carbonyl moieties, the molecules **4**−**7** in Scheme 1 were used as the coadsorbate species for a constant loading of **1** (5 m*m*) on the external surface of silicalite S1, which possesses the highest ESA per unit mass. The percentages of free components in the EPR spectra of **1** as a function of the loadings of **4**−**7**, shown in Figure 6, provide an evaluation of the relative binding strength of each coadsorbate. The percentage of the free components was evaluated by performing a subtraction−addition procedure to extract the fast and slow components from each EPR spectrum and then the double integration of the spectra gives the percentage of the two components.[20]

Several conclusions can be drawn from an examination of Figure 6. The absence of a second ortho-methyl group in **4** compared to **5** allows **4** to interact stronger with the pore openings through intercalation of the tolyl moiety in the pore openings, thus competing more effectively with the nitroxide for the interaction with the surface. Therefore, noticeably more nitroxide probes are displaced from the strong binding sites by **4** than **5** at high loadings. The *para*-substitution for the methyls in **6** allows the absorption of this ketone into the internal surface of zeolite structure and therefore it does not compete with **1** for the adsorption at the external pore sites and no free component appears with the increase in loading. The contribution of the carbonyl group of oMeDBK to the binding strength on silicalite external surface was evaluated by comparing **5** and **7** as the coadsorbate species. While **5** is capable of displacing the nitroxides, the fact that even at high loading of **7** the nitroxide EPR spectrum is essentially free from contribution from molecules undergoing fast rotational motion suggests that the presence of the carbonyl group in the ketones contributes significantly to the ketones' ability to displace nitroxide.

Characterization of the Silicalite External Surface Using a Combination of ^{14}N and ^{15}N-labeled Nitroxides. The contribution of functional groups in the nitroxide structure to its binding strength on silicalite external surface can be evaluated using functionalized nitroxides in the competitive binding experiments. We used the probes **1**, **2**, and **3** (Scheme 1) to study the interacting ability of the silicalite surface toward probes of different structure. However, the competitive binding of **1**, **2**, and **3** cannot be investigated by a simultaneous loading of these radicals, since the hyperfine lines superimpose on one another. For this reason, we used different isotopomers of the nitroxides, since the latter show distinct EPR spectra.

Nitrogen has two stable isotopes ^{14}N and ^{15}N, with natural abundances of 99.6% and 0.4%, respectively. Therefore, the nitroxide spin probes synthesized using a natural source of nitrogen will provide essentially exclusively ^{14}N-labeled species, which shows a three-line EPR spectrum due to a nuclear spin number of $I = 1$ for ^{14}N nucleus. For ^{15}N enriched nitroxide spin probes, only two lines (^{15}N nuclear spin number $I = 1/2$) contribute to the spectra. Therefore, a deoxygenated dilute nonviscous solution of a 1:1 mixture of ^{14}N, ^{15}N nitroxides shows the spectrum displayed in Figure 7, with well-resolved lines from the two nitroxides. The superhyperfine couplings (∼0.4 G) are due to the interaction of the electron spin with protons in the nitroxide molecules.[35,36]

Isotopically labeled nitroxides were employed to study the exchange between the nitroxide probes adsorbed on the external surface strong binding sites and those on the weak binding sites or in the solution phase, on a time scale of a few hours up to a day. The solid lines in Figure 8 depict the EPR spectra acquired if the activated silicalite samples were added to a mixture of **3** and **3-^{15}N** solution, allowing the two nitroxides to adsorb on the external surface concurrently and giving rise to EPR spectra characteristic of the relative loadings of the two nitroxides. The total loadings of the two nitroxides were kept constant at a low value of 10 m*m* (compared to ca. 119−149 m*m* for the complete

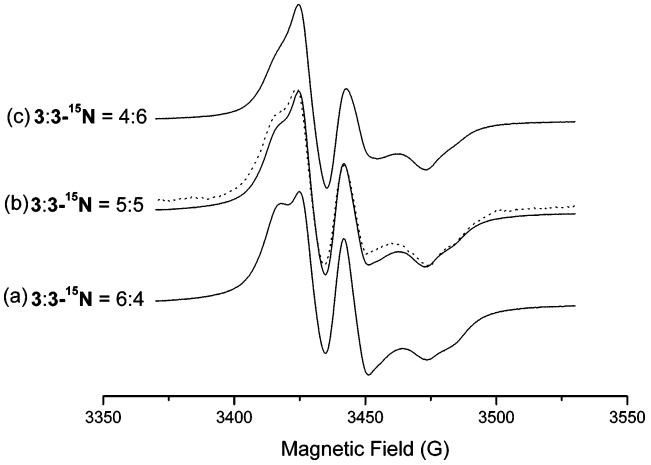

Figure 8. EPR spectra of silicalite samples loaded with **3** and **3**-^{15}**N** at different relative molar amounts on S1. Solid lines indicate concurrent loading, and dashed line indicates stepwise loading.

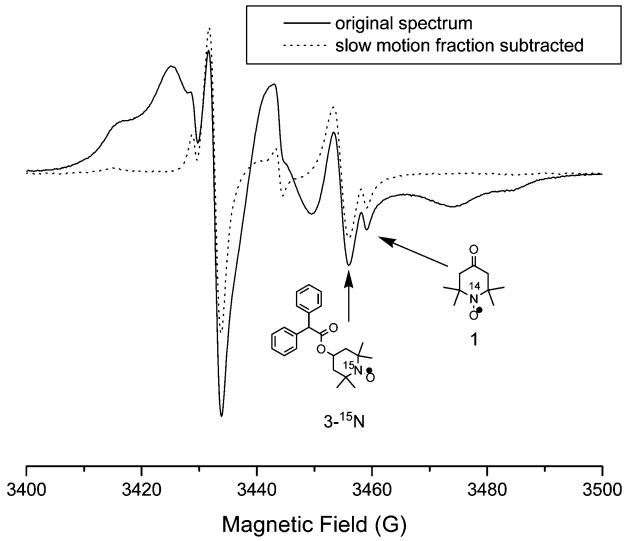

Figure 9. EPR spectrum of **1** and **3**-^{15}**N** (5 m*m* each) coadsorbed on the external surface of silicalite S1 with **4** (210 m*m*) (the solid line). The dashed line is the result of subtraction of the slow motion component from the solid line.

coverage of pore openings), ensuring an adsorption on the pore openings only. The dashed line in Figure 8 was measured on a sample with sequential loading of the two nitroxides. The adsorption equilibrium was first achieved (within a few hours) with an isooctane solution of ^{14}N-labeled probe **3** in a concentration that is more than the loading required for a complete coverage on the strong adsorption site assuming total adsorption; then, the ^{15}N-labeled probe **3**-^{15}**N** was added to the solution at the same concentration as **3** and the system was again allowed to reach equilibrium. The loaded silicalite was separated and washed with fresh isooctane before it was dried, deoxygenated, and measured in an EPR spectrometer. The EPR spectra obtained, shown as the dashed line, coincides with spectrum obtained using equal amounts of **3** and **3**-^{15}**N** loaded concurrently. It can be concluded that the stepwise loading produces a spectrum that resembles the equal loading spectrum from concurrent loading. Therefore, efficient probe exchange exists between the probes adsorbed on the strong binding sites and those in solution (or adsorbed on weak binding sites) within the time scale of a few hours up to a day.

When the coadsorbates are added at different loadings to the 1:1 mixture of the two nitroxides with exactly the same structure

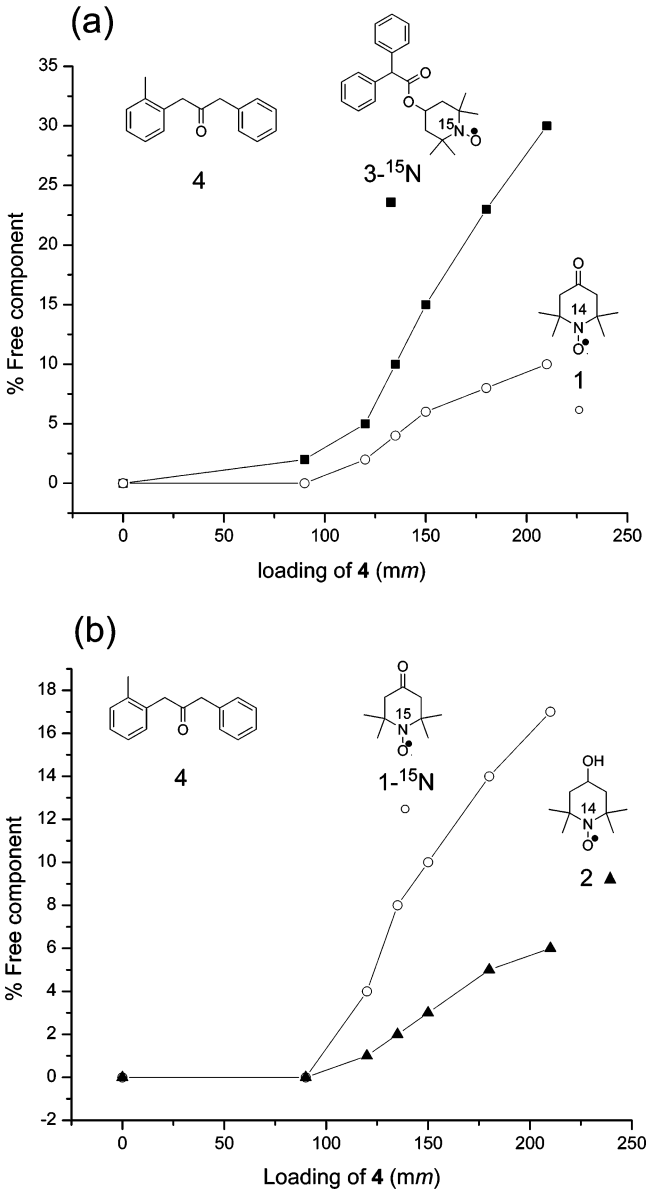

Figure 10. Percentages of nitroxides undergoing free rotational motion as a function of loading of **4** onto S1: (a) using coadsorbed nitroxides: **1** (2.5 m*m*) and **3**-^{15}**N** (2.5 m*m*); and (b) using coadsorbed nitroxides: **1**-^{15}**N** (2.5 m*m*) and **2** (2.5 m*m*).

except the nitrogen isotopes, the free components of the two isotopically labeled nitroxides appear at the same critical loading, which further depends on the structure of the nitroxide, as discussed above, and the spectrum of the free component clearly resembles the one shown in Figure 7.

The situation completely changes when nitroxides with different structures in addition to different nitrogen isotopes were coadsorbed with increasing loadings of the ketone **4**. The amount of **4** was varied to reach the onset of the nitroxide fast motion, which indicates the complete coverage of strong binding sites by **4**. However, the two radicals do not show the same amounts (percentages) of free components. Figure 9 (full line) provides an example of the EPR spectrum which was observed when **1** and **3**-^{15}**N** (1:1 ratio) are coadsorbed with **4** (210 m*m* loading) at S1 surface. Subtraction of the slow motion components gives the dotted line which clearly shows, by comparison with the spectrum in Figure 7, that the free component arising from **3**-^{15}**N** is more intense than the free component arising from **1**. Therefore, the binding of **1** is stronger than **3**-^{15}**N** on the silicalite surface strong binding sites.

The evaluation of the free component percentage of **1** and **3-^{15}N** as a function of loadings of **4** (oMeDBK) onto the external surface of S1 crystals, reported in Figure 10a, provides a quantitative measure of the more efficient displacing of **3-^{15}N** compared to **1** by oMeDBK. The reason for this disparity is easily understandable on the basis that **1** can interact more strongly with surface silanol groups than **3-^{15}N** because of the availability of a carbonyl group on the 4-position of **1**. Similarly, in Figure 10b, the variation of the free component percentage in the EPR spectra of **1-^{15}N** and **2** as a function of the loading of **4** onto S1 surface shows that **2** adsorbs on the silicalite surface more strongly than **1-^{15}N**. The stronger binding strength of **2** (4-hydroxy-TEMPO) with the strong surface binding sites is probably due to the more efficient formation of hydrogen bonding with the surface silanol groups, compared to **1** (4-oxo-TEMPO).

Conclusions

Our results demonstrate that the external surface area of a monodisperse sample of silicalite crystals and the binding strength and dynamics of organic molecules adsorbed on the silicalite external surface can be studied using EPR.

The supramolecular structure of the systems comprising organic molecules adsorbed on the silicalite external surface is coverage dependent. Low-coverage adsorption selectively occurs at the strong binding sites. After the strong binding sites are saturated, further adsorption occurs on the weak binding sites and eventually form a monolayer on the external surface of the silicalite.

Organic molecules containing a polar group in the structure adsorb stronger on the external surface than the probes with functional groups that are less polar, possibly through hydrogen bonding with surface silanols. The possible intercalation of the tolyl groups in the adsorbate structure also contributes to the binding strength on the silicalite external surface.

Using the EPR method, the silicalite's ESA can be correlated to the amount of coadsorbate molecules (EPR-silent) required to reach a certain surface coverage by following the change in the nitroxide EPR spectral parameters (e.g., rotational freedom) when some nitroxides are displaced from the strong binding sites by the coadsorbate molecules.

Using isotopically labeled nitroxides, it was concluded that the molecules adsorbed on the strong binding sites are in efficient exchange with those in the isooctane solution or on the weak binding sites on a time scale of a few hours up to a day. Isotopically labeled nitroxides can also be used in the study of structural dependence of binding strength on the zeolite external surface.

Acknowledgment. The authors at Columbia thank the National Science Foundation for its support through grant CHE01-10655 and the IUCR Center for Advanced Studies in Novel Surfactants. M.F.O. thanks the Italian Ministero per l'Universita e la Ricerca Scientifica (MIURST) for its financial support. We thank Dr. Limin Huang in Prof. Stephen O'Brien's research group at Columbia University for carrying out the XRD and SEM measurements.

Supporting Information Available: The X-ray diffraction (XRD) patterns of the silicalite samples prepared in the study are available free of charge via the Internet at http://pubs.acs.org.

References and Notes

(1) Csicsery, S. M. *Pure Appl. Chem.* **1986**, *58*, 841.
(2) Newsam, J. M. *Science* **1986**, *231*, 1093.
(3) Meier, W. M.; Olson, D. H. *Atlas of Zeolite Structure Types*, 2nd ed.; Butterworth: London, 1987.
(4) Suzuki, I.; Namba, S.; Yashima, T. *J. Catal.* **1983**, *81*, 485.
(5) Langmuir, I. *J. Am. Chem. Soc.* **1916**, *38*, 2221.
(6) Langmuir, I. *J. Am. Chem. Soc.* **1918**, *40*, 1361.
(7) Brunauer, S.; Emmett, P. H.; Teller, E. *J. Am. Chem. Soc.* **1938**, *60*, 309.
(8) Suzuki, I.; Fukuda, K. *Utsunomiya Daigaku Kyoikugakubu Kiyo, Dai-2-bu* **1983**, *33*, 23.
(9) Lippens, B. C.; de Boer, J. H. *J. Catal.* **1965**, *4*, 319.
(10) Gregg, S. J.; Sing, K. S. W. *Adsorption, Surface Area and Porosity*, 2nd ed.; Academic Press: New York, 1982.
(11) Abrams, L.; Keane, M., Jr.; Sonnichsen, G. C. *J. Catal.* **1989**, *115*, 410.
(12) Suzuki, I.; Sugaya, T. *Utsunomiya Daigaku Kyoikugakubu Kiyo, Dai-2-bu* **1988**, *38*, 31.
(13) Chu, W. C.; Chen, Y. W. *Shiyou (Taipei)* **1989**, *25*, 38.
(14) Sato, H.; Sakamoto, A.; Hirose, K.; Chikaishi, K. *Chem. Lett.* **1989**, 1695.
(15) Sayari, A.; Crusson, E.; Kaliaguine, S.; Brown, J. R. *Langmuir* **1991**, *7*, 314.
(16) Suzuki, I.; Oki, S.; Namba, S. *J. Catal.* **1986**, *100*, 219.
(17) Lunina, E. V.; Lebedeva, O. E.; Motina, A. D.; Lobza, G. V.; Latysheva, L. E.; Chenets, V. V. *Kinet. Katal.* **1987**, *28*, 1002.
(18) Li, W. Ph.D. Dissertation, Columbia University, 1999.
(19) Turro, N. J.; Lei, X.-G.; Li, W.; Liu, Z.; McDermott, A.; Ottaviani, M. F.; Abrams, L. *J. Am. Chem. Soc.* **2000**, *122*, 11649.
(20) Ottaviani, M. F.; Lei, X.-G.; Liu, Z.; Turro, N. J. *J. Phys. Chem. B* **2001**, *105*, 7954.
(21) Crea, F.; Nastro, A.; Nagy, J. B.; Aiello, R. *Zeolites* **1988**, *8*, 262.
(22) Guth, J. L.; Kessler, H.; Higel, J. M.; Lamblin, J. M.; Patarin, J.; Seive, A.; Chezeau, J. M.; Wey, R. *ACS Symposium Series* **1989**, *398*, 176.
(23) Mostowicz, R.; Crea, F.; Nagy, J. B. *Zeolites* **1993**, *13*, 678.
(24) Tavolaro, A.; Mostowicz, R.; Crea, F.; Nastro, A.; Aiello, R.; Nagy, J. B. *Zeolites* **1992**, *12*, 756.
(25) Hall, P. L.; Gilchrist, J. H.; Collum, D. B. *J. Am. Chem. Soc.* **1991**, *113*, 9571.
(26) Rauckman, E. J.; Rosen, G. M.; Abou-Donia, M. B. *Synth. Commun.* **1975**, *5*, 409.
(27) Hassner, A.; Alexanian, V. *Tetrahedron Lett.* **1978**, 4475.
(28) Turro, N. J.; Weed, G. C. *J. Am. Chem. Soc.* **1983**, *105*, 1861.
(29) Turro, N. J.; Lei, X.; Cheng, C. C.; Corbin, D. R.; Abrams, L. *J. Am. Chem. Soc.* **1985**, *107*, 5824.
(30) Jacobs, P. A.; Martens, J. A.; Weitkamp, J.; Beyer, H. K. *Faraday Discuss. Chem. Soc.* **1981**, *72*, 353.
(31) Snyder, L., R.; Kirkland Joseph, J.; Glajch, J., L. *Practical HPLC Method Development*, 2nd ed.; John Wiley & Sons: New York, 1997.
(32) Khodakov, A. Y.; Kustov, L. M.; Bondarenko, T. N.; Dergachev, A. A.; Kazanskii, V. B.; Minachev, K. M.; Borbely, G.; Beyer, H. K. *Zeolites* **1990**, *10*, 603.
(33) Tung, C.-H.; Wu, L.-Z.; Zhang, L.-P.; Li, H.-R.; Yi, X.-Y.; Song, K.; Xu, M.; Yuan, Z.-Y.; Guan, J.-Q.; Wang, H.-W.; Ying, Y.-M.; Xu, X.-H. *Pure Appl. Chem.* **2000**, *72*, 2289.
(34) Richards, R. E.; Rees, L. V. C. *Zeolites* **1988**, *8*, 35.
(35) Kreilick, R. W. *J. Chem. Phys.* **1967**, *46*, 4260.
(36) Liu, Z. Ph.D. Dissertation, Columbia University, 2003.